Trans. Inst. Indian Geographers
ISSN 0970-9851
Indexed in Scopus

Potentiality of multi-spectral remote sensing satellite sensors in geo-environmental studies: A case study of Matanomadh, Kachchh, Gujarat, Northwest India

Aditya Dharaiya*, Satyajit Gaikwad, Maharashtra; Mahesh Thakkar, Uttar Pradesh; Ramdayal Singh, Gujarat and Satish Sangode, Maharashtra

Abstract

The research examined the geo-environmental landscape of Matanomadh in Gujarat's Kachchh region, characterized by an arid climate, diverse landforms, and unique ecosystems. Using multi-spectral satellite sensors and geographic information systems, the study created detailed maps of mineralogy, land use and land cover, topography, geomorphology, and geological features. Data from sensors like Landsat, Sentinel, and Cartosat were processed to map clay mineral distribution, such as Montmorillonite, and reveal dominant barren land due to the arid climate. Topographic, geomorphological, vegetation, and hydrological maps provided insights into soil erosion and terrain impacts on ecosystems. The integration of these maps enhanced understanding of Matanomadh's geological and environmental dynamics, demonstrating the value of multi-spectral sensors and GIS for generating models like Land Cover, NDVI, MNDWI, and Mineralogy for Earth surface analysis.

Keywords: *Geospatial technology, LULC, multispectral analysis, geology, GIS*

Introduction

Geo-Environmental studies represent a multidisciplinary field that integrates geology, environmental science, and spatial analysis to understand the interactions between geological processes and environmental systems. Foundational works by Goudie (2018) has underscored the importance of studying land use, geomorphology, and topography in the context of human activities. Similarly, Gerrard and Summerfield (1992), has emphasized the role of urbanization and industrialization in reshaping landscapes, calling for sustainable approaches to mitigate their adverse environmental impacts. A growing body of literature has explored how geo-environmental research supports climate adaptation strategies and sustainable development by analysing earth surface processes and human-environment interactions (Shandilya *et al.*, 2021). However, despite these advancements, region-specific studies, especially in ecologically sensitive and geologically and geomorphologically diverse areas like Kachchh, remain limited.

Technological progress in remote sensing has significantly enhanced the capacity to monitor and assess environmental change (Hassan *et al.*, 2022). Integration of remote sensing data with GIS and machine learning

tools has enabled more sophisticated analysis and modelling of environmental phenomena like urban sprawl, deforestation, and hazard susceptibility; yet, the application of such advanced techniques remains underutilized in semi-arid and ecologically fragile regions like Kachchh.

Kachchh, located in Gujarat, India, offers a distinct geo-environmental setting marked by arid climatic conditions, variable topography, and rich but fragile ecosystems. Previous studies have addressed issues like desertification, salinity ingress, and climate variability in this region (Rani & Paul, 2023). The degradation of the Banni grasslands shrinking from around 3,800 to 2,600 km^2 is a key indicator of desertification, driven by overgrazing, land-use changes, and the invasive spread of *Prosopis juliflora* (Mathur & Sharma, 2018). This ecological imbalance is further compounded by recurring droughts, with 48 out of 82 years between 1932 and 2013 marked by drought conditions. Simultaneously, climate change has led to erratic rainfall patterns, a significant increase in average seasonal rainfall (from 378 mm to 674 mm between 1984 and 2013), more frequent and intense cyclones in the Arabian sea, and a rising occurrence of heatwaves (Kumar *et al.*, 2015).

There is a noticeable gap in the localized application of integrated remote sensing, GIS, and machine learning approaches to analyse micro-level geo-environmental characteristics. This study aims to address this gap by leveraging high-resolution spatial data and advanced analytical techniques to evaluate the geo-environmental dynamics of the Matanomadh area. The study aims of demonstrating how multispectral satellite remote sensing when integrated with Machine Learning approaches can effectively map clay minerals, land use/land cover, topography and geomorphology to evaluate the geological and environmental framework of Matanomadh within the broader context of semi-arid landscapes.

Geological setting of Matanomadh

Matanomadh, a village in Lakhpat Taluka of Kachchh district, Gujarat, India, lies between 22.54° to 22.56°N and 68.95° to 68.97°E (Fig. 1). It is nestled in a valley surrounded by hills with a small stream flowing through it. The Kachchh Basin, a peri-cratonic rift basin on India's western edge, holds an almost continuous geological sequence from the Triassic to the present, although some gaps exist between transgression cycles. The western Kachchh region predominantly exposes Tertiary formations, and the basin itself formed due to the Gondwana breakup during the Late Triassic to Early Jurassic (Bhosale *et al.*, 2021; Biswas, 2016). This basin, located within the Mid-Proterozoic Aravalli-Delhi fold belt, developed along the southern Indus shelf, which was submerged by the Mid-Jurassic Period (Patel *et al.*, 2010). The Matanomadh Formation, part of the Paleocene Madh Series, features unique mineral assemblages in its altered basalts and sedimentary sequences deposited in a shallow marine environment, overlying Mesozoic formations and indicating pre-tectonic activity (Biswas, 2016; Biswas & Chauhan, 2016). This assemblage includes jarosite, hydrous sulphates, kaolinite, and Fe/Mg smectites (Bhattacharya *et al.*, 2016), reflecting complex hydrothermal and weathering processes. The geological map of the Matanomadh area (Fig. 2) highlights various lithostratigraphic units, including Eocene-aged Kakdi Nadi formation,

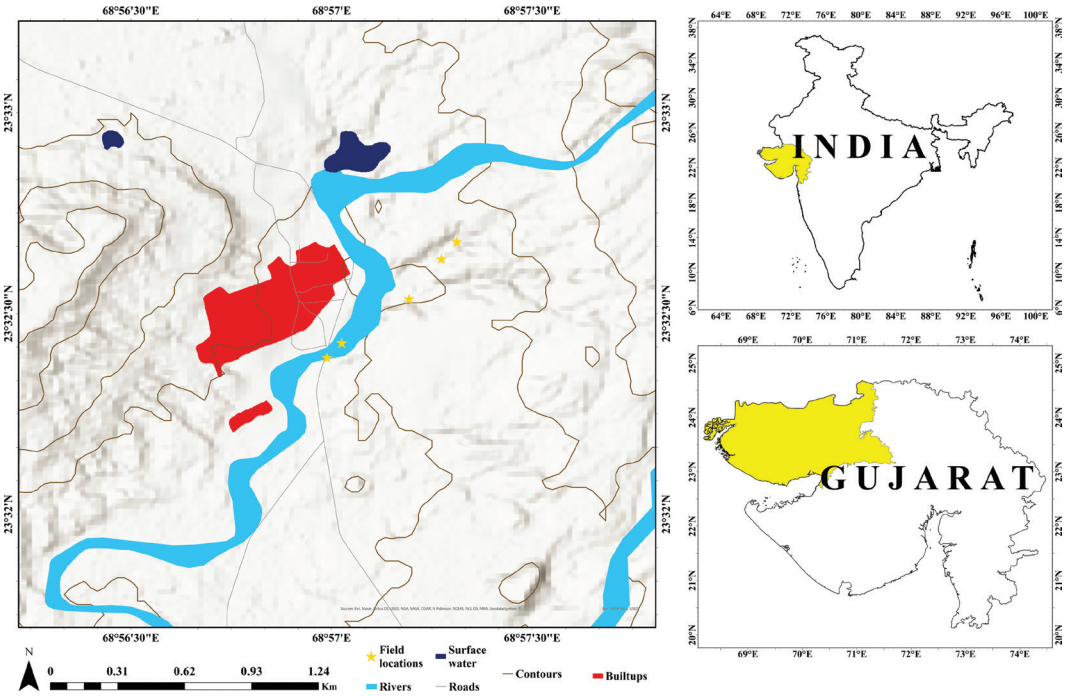

Fig. 1: Location and topography of Matanomadh area.

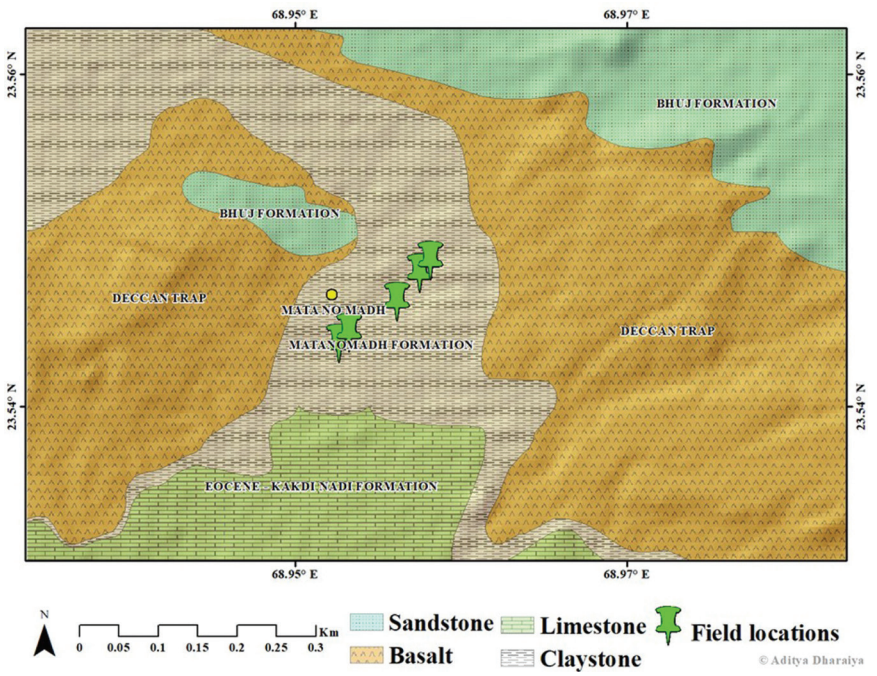

Fig. 2: Lithostratigraphic formations around Matanomadh

Cretaceous Trap basalts, and the Paleocene Matanomadh formation in the central portion of the village.

Materials and methods

Data acquisition

Geological mapping of the Matanomadh area utilized Survey of India (SOI) toposheet (41A/14, 1:50,000 scale) and Geological Survey of India (GSI) maps for Paleocene and Eocene formations. Digital elevation map (DEM) data from Cartosat-1 (via BHUVAN ISRO) aided in topographical analysis, while land use layers were digitized using OpenStreetMap on QGIS. Satellite imagery from SENTINEL-2A (ESA) and cloud-free LANDSAT 8 OLI (USGS) of the time period of March 2023, provided necessary spectral and spatial data for the study.

Field survey

The site was carefully explored with the intention of documenting various rock outcrops and sedimentary structures during traverses conducted in the field (Fig. 3). The field survey was conducted once in two years for four days during March–June. Throughout the survey, features such as joints and cross beddings, which provided valuable insights into the geological characteristics of the area were observed. Alongside, the land use and land cover features, geological, topographical features were thoroughly examined and performed a ground-truthing using a random sampling strategy in order to perform accuracy assessment to verify the LULC outcome of remote sensing.

Methodology

Data pre-processing: Remote sensing data was processed using ArcGIS 10.8® and QGIS 3.28.4, utilizing the QuickOSM plugin to download OSM land use data as vector layers. Cartosat-1 DEM images were mosaicked in ArcGIS, clipped to the area of interest, and processed with hill-shade and contour tools to create a 3D textured map and 20 cm interval contours. The SOI toposheet (41A/14) was georeferenced, digitized, and classified based on lithological features to produce a geological map of the Matanomadh.

Band combinations: Landsat and Sentinel satellites capture multispectral imagery, enabling feature analysis by combining bands. True-colour composites use bands 4, 3, and 2 in both satellites. NIR false-colour composites (e.g., Landsat 5, 4, 3; Sentinel-2 8, 4, 3) enhance vegetation, appearing bright red, aiding in monitoring health and density SWIR bands (e.g., Landsat 6, 7; Sentinel-2 11, 12) are used to analyze moisture content and identify rock types.

Band ratios: Vegetation indices, such as the Normalized Difference Vegetation Index (NDVI) and Modified Normalized Difference Water Index (MNDWI), combine spectral bands like red, near-infrared (NIR), and blue to evaluate vegetation health, density, and moisture content, aiding ecosystem management. *The formulae for both of these are shown below*:

$$NDVI = (\rho NIR - \rho RED) / (\rho NIR + \rho RED)$$

For Sentinel 2A, NDVI = Band 8 − Band 4 / Band 8 + Band 4

$$MNDWI = \rho GREEN - \rho SWIR / \rho GREEN + \rho SWIR$$

For Sentinel 2A, MNDWI = Band 3 − Band 11 / Band 3 + Band 11

The band ratio method is a key remote sensing technique for geological studies, where ratios of reflectance values from

different spectral bands highlight specific minerals. For identifying clay minerals like Gibbsite, Kaolinite, and Smectite, shortwave infrared (SWIR) bands are effective due to their high absorptivity. In this study, Landsat 8 OLI bands 7 and 6, and Sentinel-2A bands 12 and 11 were ratioed using GIS software. The vegetation and clay index for Landsat-8 was derived from the 6/7 and 5/4 band ratios, while the Sentinel-2A clay index used the 12/13 and 8/4 ratios, respectively. Thus, band ratio 4/2 was used to superpose vegetation + clays for both LANDSAT & SENTINEL. Clay minerals such as montmorillonite, kaolinite, and illite exhibit distinct absorption features in the SWIR region (approximately 1.5–2.3 μm) due to their hydroxyl (OH-) and metal–OH bond vibrations. Band combinations like Landsat 7 band 7 (SWIR2: 2.08–2.35 μm) / band 5 (NIR: 0.85–0.88 μm) and Sentinel-2 band 12 (SWIR: 2.10–2.29 μm) / band 8A (NIR: 0.86–0.88 μm) effectively highlight the presence of these minerals. (Ducart, *et al.*, 2016).

Supervised classification: It is a process of training a computer algorithm to recognize and differentiate between different objects or land cover types within an image. A set of training samples was prepared as a signature file for the different LULC features and clay minerals. Based on the respective spectral signatures of the various objects and features, the Maximum Likelihood Algorithm was processed, thus to classify the LULC classes and to detect the clay mineral patches within the Matanomadh.

Accuracy assessment: An error matrix, also known as a confusion matrix, was prepared which is a fundamental tool for assessing the accuracy of classification results. With the help of sampling strategy used in the field corresponding to the classes created using supervised classification, the overall accuracy and kappa coefficient was calculated using the following formulae (*Cohen, 1960*):

Overall accuracy = Total Corrected Samples (TCS) / Total Samples (TS) * 100

Kappa Coefficient (T) = (TS * TCS) – Σ (Column Total * Row Total) / TS^2 – Σ (Column Total * Row Total)

Spatial overlay analysis: Raster overlay is a type of overlay analysis in GIS that involves combining and analysing raster datasets or layers. Raster overlay is particularly useful for analysing continuous data such as elevation, temperature, land cover, and satellite imagery. In the present study, the outputs generated through Band ratios of SENTINEL 2A and LANDSAT 8 OLI along with the supervised classification of SENTINEL 2A geological band combination was overlaid in the software. Then, the respective clay formation or clay patches in the Matanomadh were extracted through this overlay analysis of three preliminary results. For accuracy purpose, the remotely sensed output data was thus confirmed by a field visit.

The overall methodology adopted for the research is presented in a flow chart in figure 4.

Results

The key elements of the results of the analysis is presented below:

Clay mineral mapping

By implementing the maximum likelihood algorithm in Geological FCC of SENTINEL 2A, the classification process accurately identified and delineated areas within the imagery that corresponded to clay and

Fig. 3: Geological field sites observed in the Matanomadh area.

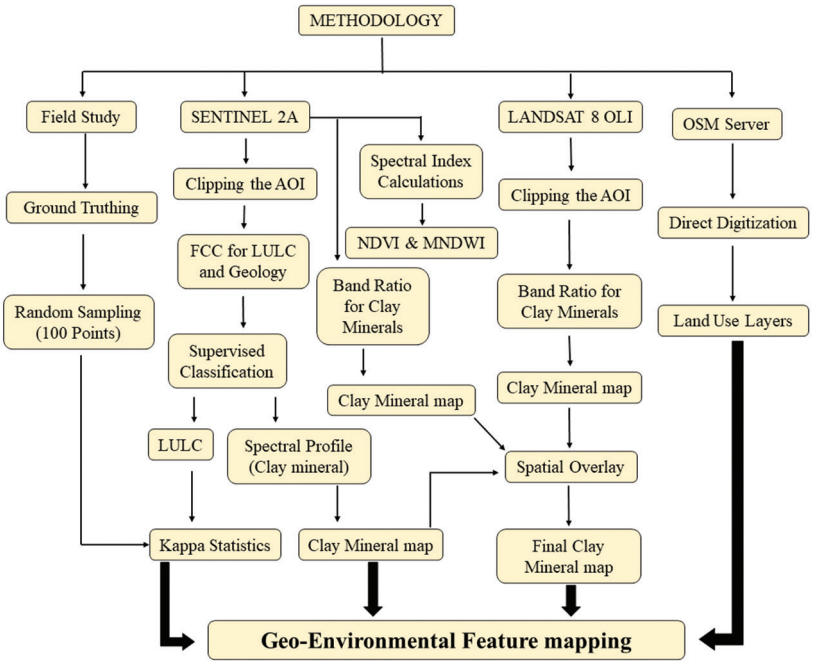

Fig. 4: Flow diagram of the methodology carried out in the study.

carbonate minerals, confirmed during the field work. These areas were isolated for separate identification and mapping. The results of the classification provided the spectral distribution of clay and carbonate areas within the Matanomadh which is shown as spectral profile (Fig. 8). The profile shows the diagnostic absorption features of clay minerals, particularly Montmorillonite (Smectite) in the shortwave infrared (SWIR) region (1.5–2.3 μm). The reflectance curves dip at specific SWIR wavelengths due to the –OH bond vibrations and metal–OH combinations present in clays such as montmorillonite, kaolinite, and illite. These absorptions make them spectrally distinct from surrounding barren land, vegetation, or carbonate surfaces. *The classification map*

Table 1: Error matrix for land use and land cover classification

Class	Barren	Built-up area	Mining area	Vegetation	Water body	Total (User)
Barrens	18	1	0	1	0	20
Built-up area	3	15	2	0	0	20
Mining area	0	2	18	0	0	20
Vegetation	1	0	0	18	1	20
Water body	0	0	0	0	20	20
Total (Producer)	22	18	20	19	21	100

Overall accuracy = 89%, Kappa (T) = 0.8

Table 2: User and producer accuracy (UA & PA) of each representative LULC class.

Class Name	User's Accuracy (%)	Producer's Accuracy (%)
Barrens	18/20 = 90%	18/22 = 81.8%
Built-up	15/20 = 75%	15/18 = 83.3%
Mining area	18/20 = 90%	18/20 = 90.0%
Vegetation	18/20 = 90%	18/19 = 94.7%
Water body	20/20 = 100%	20/21 = 95.2%

further highlighted the extent and boundaries of these mineral-rich regions.

Land use and land cover

Using Maximum Likelihood Algorithm in LULC, FCC of SENTINEL 2A identified five distinct land cover classes in the Matanomadh of approximately 18 km²: Barrens, Built-up area, Mining area, Vegetation, and Water body (Fig. 5). The Barrens, areas with sparse or no vegetation, covers approximately 9.5 km². The Built-up areas with human infrastructure and urban development spans about 1.25 km². The Areas of active mining or extraction industries covered some 0.2 km². Vegetation including forests, grasslands, and agricultural fields extends over 7.25 km². Water bodies cover 0.25 km², including rivers, lakes, or other water sources.

To assess the accuracy of the LULC classification from Sentinel 2A imagery, an error matrix was generated using 100 random sampling points using the Equalized Stratified Random Sampling strategy (Table 1). The analysis revealed an overall accuracy of 89%, indicating that 89 out of 100 sample points were correctly classified. This demonstrates a high level of precision in the classification results. From Table 2, the classification demonstrates high reliability across most land cover classes, with particularly strong performance for Water bodies (100% user accuracy, 95.2% producer accuracy) and Vegetation (90% UA, 94.7% PA), indicating clear spectral separability. Mining areas also show high accuracy (90% UA and PA), while Barrens and Built-up areas exhibit slightly lower accuracies due to spectral confusion, likely caused by overlap with adjacent land cover types or mixed pixels.

Additionally, the Kappa Coefficient, a statistical measure that accounts for agreement by chance, was calculated to further evaluate the reliability of the classification. The Kappa co-efficient for this classification was 0.8, indicating strong agreement between the classified imagery and reference data. A Kappa value of 0.8 suggests near-perfect accuracy with minimal error. In summary, the LULC classification of Sentinel 2A imagery achieved high reliability, with an overall accuracy of 89% and a Kappa Coefficient of 0.8, highlighting the effectiveness of the classification process. The potential sources of errors can be due to spectral mixing of land cover classes resulting into ambiguous spectral signatures and can be due to sensor radiometric calibration issues.

Topographical mapping

The topographical map of the Matanomadh area in Kachchh (Fig. 1) shows the elevated areas using 20m interval contours in and around Matanomadh. In addition to the elevation information, the topographical map also incorporates other essential features.

Surface water bodies, such as rivers, lakes, or reservoirs, are clearly depicted, providing insights into the hydrological network of the area. The slope analysis reveals steep gradients along valley margins and gentler slopes transitioning into pediplains. River networks and surface water bodies are distinctly mapped, showing small streams and catchments that define the local watershed pattern. Water resources are primarily confined to low-lying depressions and valley floors where small streams and reservoirs occur. River channels mapped across the terrain highlight the natural flow directions and catchment zones, reflecting areas of surface water concentration. Steeper upland zones promote rapid runoff and limit water retention, while gentler pediplains provide favourable conditions for groundwater recharge and localized storage.

Geomorphological mapping

The Matanomadh area in Kachchh showcases a variety of geomorphological features that shape its distinctive landscape. Key features include a dissected plateau, pediments (i.e., erosional slope), pediplains (i.e., erosional plains), and water bodies (Fig. 6). The dissected plateau, located in the northeast and southwest, consists of elevated landforms eroded by deep valleys and ravines, creating rugged terrain with steep slopes and complex drainage patterns. In the central region, pediments gently sloping surfaces at the base of hills serve as transitional zones between higher elevations and adjacent low-lying plains, formed by erosion and sediment deposition. Additionally, the Matanomadh area contains a pediplain complex, characterized by vast, gently sloping plains developed through prolonged erosion in arid or semi-arid conditions. These smooth, undulating surfaces often have a thin sediment cover and reflect extensive weathering processes. Together, these landforms highlight the dynamic processes of erosion, deposition, and weathering that have shaped the region over time.

Band ratio results

Clay mineral mapping: The Band ratio method was successfully applied to both LANDSAT and SENTINEL satellite data for the purpose of detecting clay and carbonate minerals in Matanomadh (Fig. 7). These results were generated using the calculation of spectral band ratios using specific SWIR bands sensitive to the spectral signatures of these minerals.

By analysing the band ratios derived from the satellite images, distinct spectral characteristics associated with clay and carbonate minerals were identified and can be seen as a spectral profile of these minerals generated using the software (Fig 8). These spectral plots were compared using USGS spectral plots library. The results show the spatial distribution and abundance of clay and carbonate minerals in Matanomadh, shown in Fig. 7 where, clay and carbonate mineral hotspot occurrences were identified, showing areas with higher concentration or favourable conditions for the formation of these minerals.

NDVI and MNDWI

In the Matanomadh Region, the maximum observed NDVI value is +0.5, indicating sparse vegetation, likely affected by environmental conditions. Most of the NDVI values in the region are negative, reflecting moisture-rich areas, possibly due to the dominance of clayey lithologies that retain moisture (Fig. 9). This mix of

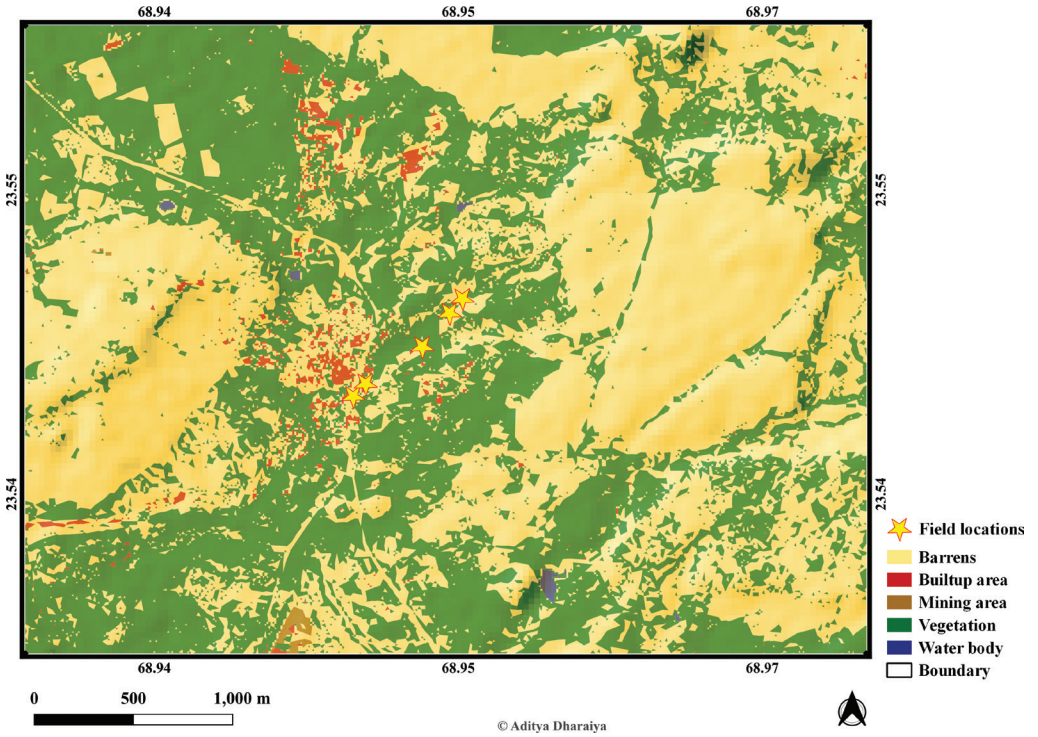

Fig. 5: Land use and land cover features in Matanomadh

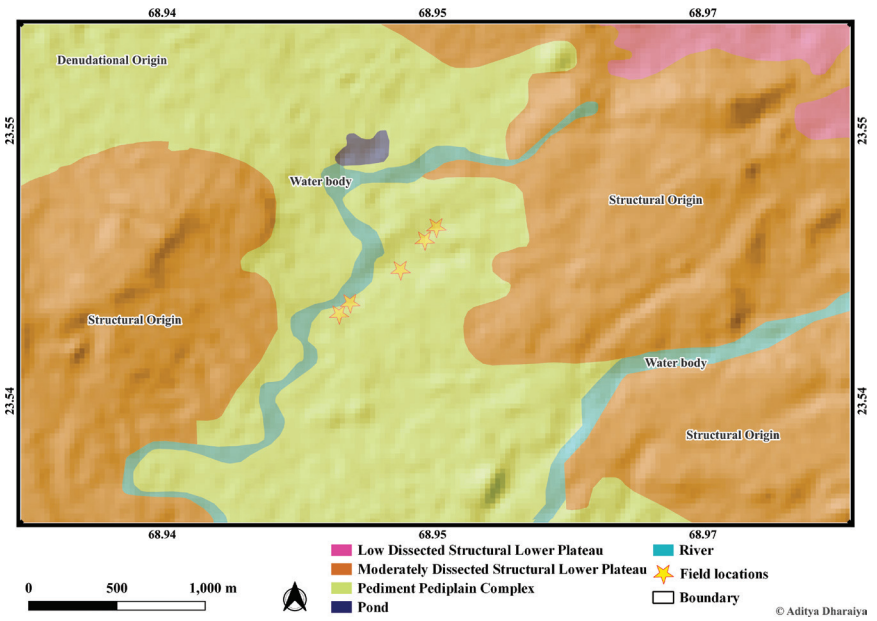

Fig. 6: Tectono-geomorphic map of Matanomadh

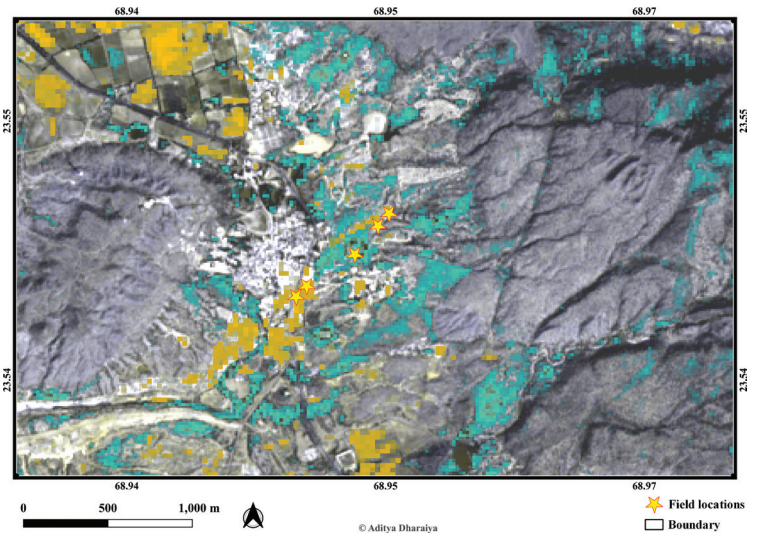

Fig. 7: distribution of clay minerals in Matanomadh, mapped using band ratio methods from Landsat 8 OLI and Sentinel-2 imagery. The approach utilizes the distinct SWIR absorption features of clay minerals to identify clay-rich zones, with combined satellite data enhancing detection accuracy.

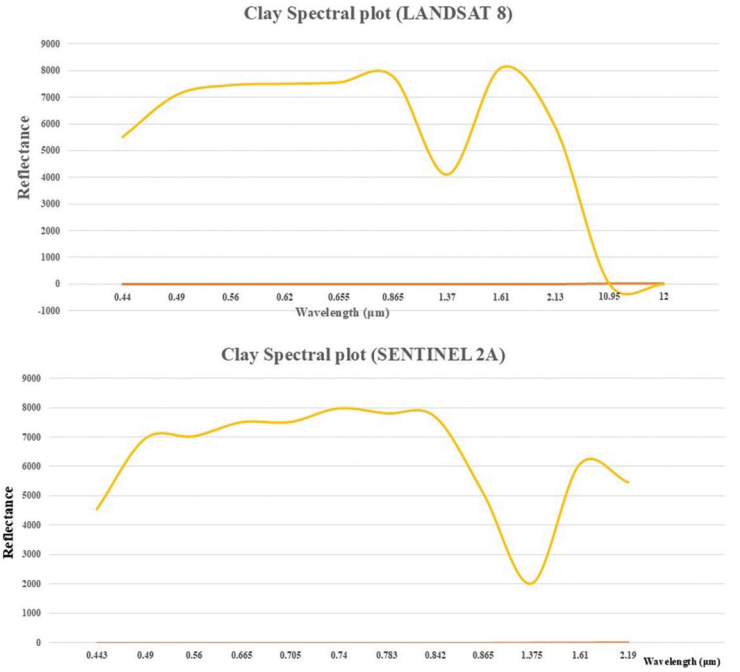

Fig. 8: Spectral reflectance plots of Montmorillonite clay mineral generated in QGIS using Landsat 8 OLI and Sentinel-2A imagery. The plots highlight key absorption features in the SWIR region (1.5–2.3 µm), confirming the suitability of Landsat bands 6/7 and Sentinel bands 11/12 for clay mineral detection.

sparse vegetation and significant moisture retention highlights the unique environmental characteristics of the region. In comparison, arid zones like the Thar desert often report (Karnieli *et al*., 2001) higher NDVI thresholds for sparse to moderate vegetation (+0.3 to +0.6) due to slightly denser seasonal vegetation or different spectral properties of the land surface.

In the Matanomadh region, the maximum MNDWI value is +0.36, suggesting water bodies are contaminated with fine sediments, such as silt and clay, common in the area. Moderate MNDWI values indicate the presence of water with lower clarity, while values near zero represent moisture-retaining areas like wet soils or mudflats. Negative MNDWI values likely correspond to vegetation (Fig. 9). MNDWI values for clean, deep-water bodies generally exceed +0.5, while sediment-laden or turbid waters register lower, typically between +0.2 and +0.4. This analysis reflects the interaction between water, moist areas, and vegetation, shaping the MNDWI values across the landscape.

The Sentinel-2A imagery from March 2023 captures conditions during a transitional period in arid regions, typically following winter rains. This timing can result in slightly elevated NDVI values due to brief vegetation activity, although overall vegetation remains sparse. Similarly, MNDWI values may reflect ephemeral water bodies or increased soil moisture, common after seasonal precipitation thus, enhances detection of sparse vegetation, moist clay-rich soils, and potential water contamination, these indices are highly sensitive to seasonal variability.

Spatial overlay results

Overlay analysis was conducted to generate a spatial distribution map of clay-rich areas in and around Matanomadh, using a combination of supervised clay classification and band ratios derived from LANDSAT and SENTINEL satellite images. The supervised clay classification, based on the maximum likelihood algorithm, provided accurate identification of clay-rich areas within the Matanomadh, which covers about 110 Km^2. This classification was derived from spectral signatures and reflectance values specific to clay and carbonate minerals. The resulting clay classification map served as the base layer for subsequent analysis.

The band ratios derived from LANDSAT and SENTINEL images were utilized in the overlay analysis. Band ratios are calculated using specific bands that are sensitive to the spectral signatures of clay and carbonate minerals. The result of the overlaying of these band ratios with the classified clay map is the accurate spatial distribution of clay-rich areas (Fig. 10). The overlay analysis produced a comprehensive clay distribution map, highlighting the precise spatial extent of clay-rich areas/patches in and around Matanomadh.

Discussion

The integration of multispectral remote sensing, particularly through Landsat-8 band ratio indices, has proven to be a powerful tool for mapping clay minerals and assessing environmental features in diverse geological settings. In this study, the use of Landsat-8's spectral capabilities, especially in the shortwave infrared (SWIR) region, enabled the successful detection of Montmorillonite-a key smectite-group clay mineral within the arid terrain of the Matanomadh region in Kachchh. This is consistent with previous similar studies that have leveraged SWIR data to map similar clay mineral assemblages

in arid and semi-arid Saharan environments in Algeria (Grandjean *et al*., 2010), the Thar Desert (Chattoraj *et al*., 2020), and parts of Central Iran (Gad & Kusky, 2006).

Our study also revealed that the Matanomadh region is predominantly characterized by barren land and sparse vegetation, as indicated by low NDVI values. These findings align with patterns observed in arid Thar desert in India and regions of northern Mexico (Gallardo-Salazar *et al*., 2023), where remote sensing has been used to classify sparse or degraded vegetation cover and monitor desertification trends and NDVI has been used to track the dynamics of arid-land vegetation and land degradation. Similarly, the presence of contaminated water bodies, identified through negative MNDWI values, reflects environmental stress conditions likely linked to both anthropogenic impacts and natural hydrological constraints (Grandjean *et al*., 2019).

The applications of these indices proved instrumental in identifying regions of ecological degradation, environmental stress, and water scarcity. These indices not only confirmed the prevalence of sparse vegetation and water stress in Matanomadh but also illustrated the utility of satellite-based indices in monitoring land use changes and ecosystem health over time.

Sentinel-2, with its higher spatial resolution and broader spectral coverage, further enhanced the analysis, allowing for better land cover classification and environmental monitoring, by generating a high quality, resolution and accuracy map products, which precisely detected the land use and land cover classes on a larger scale. When combined with Landsat-8, the synergy between these two platforms allowed for more accurate detection of geomorphological features, such as dissected plains/plateaus and pediment-pediplain complex, and more precise mapping of surface compositions.

In this study, spectral analysis of Landsat-8 and Sentinel-2 data successfully mapped clay minerals such as kaolinite, smectite, and illite within the Matanomadh region. The results confirmed the dominance of Montmorillonite-rich patches in clay-bearing zones, consistent with field observations and spectral profile validation (Saadat *et al*., 2023). The fusion of machine learning and GIS with remote sensing data also offered significant advantages by enhancing the precision of classification and improving the detection of subtle spectral variations in complex arid terrains. Machine learning algorithms allowed better differentiation of overlapping land cover classes, reducing classification errors, while GIS-based spatial analyses integrated these results to delineate mineral-rich zones and geomorphological features more accurately.

Conclusion

This study demonstrated that the integration of multispectral satellite data with GIS provides a robust framework for understanding the geo-environmental dynamics of the Matanomadh region in Kachchh. The results highlight that land use and land cover is dominated by barren land and sparse vegetation, confirmed by NDVI values, while water resources are limited and largely confined to drainage lines and low-lying depressions, as reflected in MNDWI analysis. Clay mineral mapping, supported by band ratios and spectral profiles, successfully delineated montmorillonite- and carbonate-rich zones, validated through field observations, thus underscoring the potential of SWIR-based remote sensing

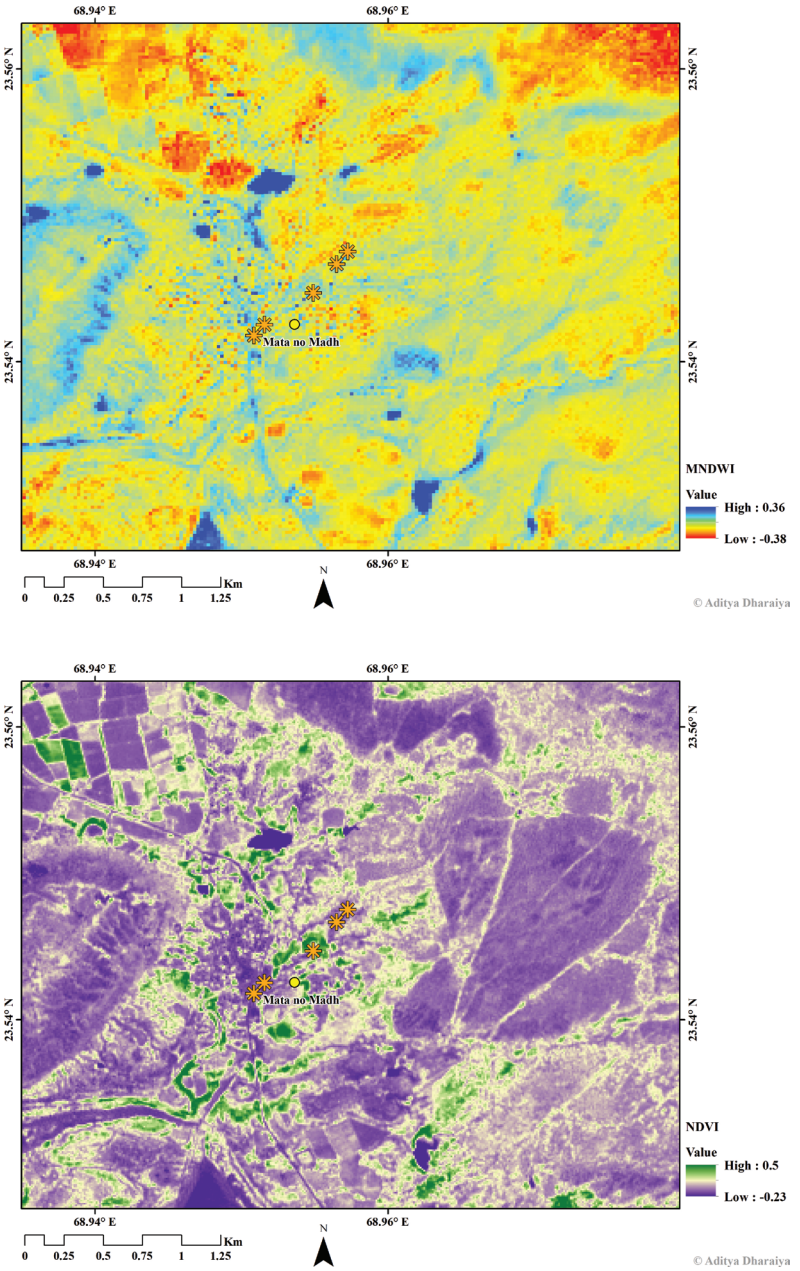

Fig. 9: Distribution of vegetation, water bodies, and surface moisture in the Matanomadh, derived from MNDWI and NDVI indices. It highlights sparse vegetation typical of the arid region and captures both permanent and temporary water sources, offering key insights for ecological and water resource management.

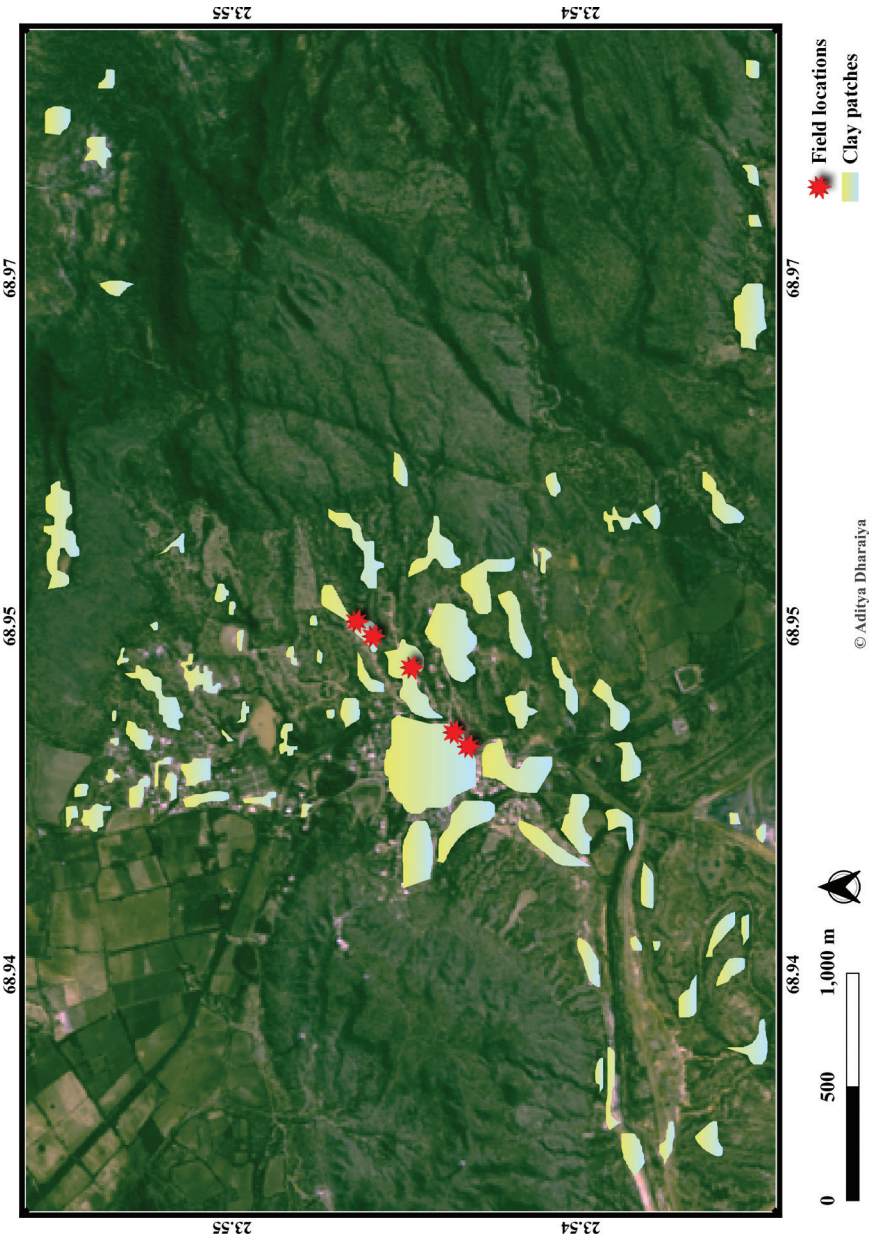

Fig. 10: Spatial distribution of clay mineral patches primarily Montmorillonite identified within the 4 km^2 of Matanomadh using overlay analysis of Landsat-8 SWIR band ratios and Sentinel-2 imagery. The mapped patches highlight zones of clay-rich deposits, particularly concentrated in geologically exposed or weathered regions, indicative of past hydrothermal or Pedogenic processes.

for mineralogical studies in semi-arid terrains. Topographic and geomorphological mapping revealed the interplay between rugged uplands, pediments, and pediplains, controlling river networks and water availability. Together, these results provide a comprehensive synthesis of how geology, landforms, vegetation, water, and mineral resources interact under arid environmental conditions. Beyond scientific outcomes, the approach also aligns with SDG 4 (quality education) by fostering accessible, data-driven tools for earth science learning and promoting geoscience literacy to address environmental challenges.

However, remote sensing methods are constrained by atmospheric interference, sensor resolution, and spectral overlap among minerals, while seasonal variability can affect vegetation and water index results. Ground validation, though conducted, was limited in temporal scope, and future work should integrate hyperspectral datasets, and time-series monitoring for greater accuracy. Moreover, bio-signature studies in clay minerals offer promising avenues for astrobiology and habitability research.

Looking ahead, expanding such research will not only refine clay mineral detection and bio-signature exploration but also strengthen conservation frameworks. The Matanomadh formation, with its unique mineralogical and geo-environmental heritage, represents a valuable geo-heritage site that requires urgent preservation, protection, and community-driven conservation. Safeguarding such sites will ensure that their scientific, cultural, and educational values are sustained for future generations, while also reinforcing the role of geo-environmental research in global sustainability efforts.

Competing interest

The corresponding author declares that they have no conflict of interest.

References

Ben-Dor, E., Chabrillat, S., & Demattê, J. A. (2018). Characterization of soil properties using reflectance spectroscopy. *Fundamentals, sensor systems, spectral libraries, and data mining for vegetation, CRC Press*. 187-247. https://doi.org/10.1201/9781315164151-8.

Bhattacharya, S., Mitra, S., Gupta, S., Jain, N., Chauhan, P., & Parthasarathy, G. (2016). Jarosite occurrence in the Deccan Volcanic Province of Kachchh, western India: Spectroscopic studies on a Martian analog locality. *Journal of Geophysical Research: Planets, 121*, 402–431. https://doi.org/10.1038/175238c0.

Bhosale, S., Chaskar, K., Pandey, D. K., Lakhote, A., Thakkar, A., Chauhan, G., Bhandari, S., & Thakkar, M. G. (2021). Jurassic geodiversity and geomorphosite of Kanthkot area, Wagad, Kachchh, Western India. *International Journal of Geoheritage and Parks, 9*(1), 51–68. https://doi.org/10.1016/j.ijgeop.2020.12.008.

Biswas, S. K. (2016). Mesozoic and tertiary stratigraphy of Kutch (Kachchh)–a review. *In Conference GSI*. 1–24. https://doi.org/10.17491/cgsi/2016/105405.

Biswas, S. K., & Chauhan, G. (2016). The Kutch Rift Basin –Potential Location For A National Geopark Of India S. *Potential Geoparks of India*, 1–36.

Chattoraj, S. L., Prasad, G., Sharma, R. U., Ray, C. P. K., van der Meer, F. D., Guha, A., & Pour, A. B. (2020). Integration of remote sensing, gravity and geochemical data for exploration of Cu-mineralization in Alwar basin, Rajasthan, India. *International Journal of Applied Earth Observation and Geoinformation, 91*, 102162. https://doi.org/10.1016/j.jag.2020.102162.

Cohen, J. (1960). A Coefficient Of Agreement For Nominal Scales. *Educational and Psychological Measurement, XX*(1), 37–46. https://doi.org/10.1177/001316446002000104.

Ducart, D. F., Silva, A. M., Toledo, C. L. B., & Assis, L. M. D. (2016). Mapping iron oxides with Landsat-8/OLI and EO-1/Hyperion imagery from the Serra Norte iron deposits in the Carajás Mineral Province, Brazil. *Brazilian Journal of Geology, 46*(03), 331-349. https://doi.org/10.1590/2317-4889201620160023.

Gad, S., & Kusky, T. (2006). Lithological mapping in the Eastern Desert of Egypt, the Barramiya area, using Landsat thematic mapper (TM). *Journal of African Earth Sciences, 44*(2), 196-202. https://doi.org/10.1016/j.jafrearsci.2005.10.014.

Gallardo-Salazar, J. L., Rosas-Chavoya, M., Pompa-García, M., López-Serrano, P. M., García-Montiel, E., Meléndez-Soto, A., & Jiménez-Jiménez, S. I. (2023). Multi-temporal NDVI analysis using UAV images of tree crowns in a northern Mexican pine-oak forest. *Journal of Forestry Research, 34*(6), 1855–1867. https://doi.org/10.1007/s11676-023-01639.

Gerrard, J., & Summerfield, M. A. (1992). Global Geomorphology: An Introduction to the Study of Landforms. *The Geographical Journal, 158*(1), 100. https://doi.org/10.2307/3060043.

Goudie, A. S. (2018). Human impact on the natural environment. *John Wiley & Sons*. https://thuvienso.hoasen.edu.vn/bitstream/handle/123456789/10554/Contents.pdf?sequence=5&isAllowed=y.

Grandjean, G., Briottet, X., Adeline, K., Bourguignon, A., Grandjean, G., Briottet, X., Adeline, K., Hadeel, A.S., Jabbar, M. T., & Chen, X. (2010). Application of remote sensing and GIS in the study of environmental sensitivity to desertification: a case study in Basrah Province, southern part of Iraq. *Appl Geomat, 2*, 101–112. https://doi.org/10.1007/s12518-010-0024-y.

Hasan, M. Z., Leya, R. S., & Islam, K. S. (2022). Comparative assessment of machine learning algorithms for land use and land cover classification using multispectral remote sensing image. *Khulna University Studies*, 33-46. https://doi.org/10.53808/KUS.2022.ICSTEM4IR.0124-se.

Karnieli, A., Kaufman, Y. J., Remer, L., & Wald, A. (2001). AFRI Aerosol free vegetation index. *Remote Sensing of Environment, 77*(1), 10-21. https://doi.org/10.1016/S0034-4257(01)00190-0.

Kumar, V. V., Mahato, A., & Patel, R. (2015). Ecology and management of Banni grassland of Kachchh Gujarat. *Ecology and management of grassland habitats in India, 17*, 42-53.

Mathur, M., & Sharma, K. (2018). Modelling the economics of grassland degradation in Banni, India, using system dynamics. *Ecology,*

Economy and Society–the INSEE Journal, 1(2), 31-65. https://doi.org/10.37773/ees.v1i2.34.

Rani, J. & Paul, B. (2023). Challenges in arid region reclamation with special reference to Indian Thar Desert—its conservation and remediation techniques. *International Journal of Environmental Science and Technology, 20*(11), 12753-12774. https://doi.org/10.1007/s13762-022-04746-z.

Saadat, S., Ghoorchi, M. & Dabiri, R. (2023). Extracting clay minerals with emphasis on Bentonite in Eastern Iran, using Landsat 8 and ASTER images. *Iranian Journal of Earth Sciences, 15*(3), 188-194. https://doi.org/10.30495/ijes.2023.1973739.1815.

Shandilya, A. K., Singh, V. K., Bhatt, S. C., & Dubey, C. S. (Eds.). (2021). Geological and geo-environmental processes on earth. *Springer Nature*. 1-4. https://www.academia.edu/download/115461441/ 978-981-16-4122-0_1.pdf.

Wang, Z., Shi, Y., & Zhang, Y. (2023). Review of desert mobility assessment and desertification monitoring based on remote sensing. *Remote Sensing, 15*(18), 4412. https://doi.org/10.3390/rs15184412.

Aditya Dharaiya*
Research Student,
Department of Geology,
Savitribai Phule Pune University,
Pune, Maharashtra

Satyajit Gaikwad
Professor,
Department of Geology,
Savitribai Phule Pune University,
Pune, Maharashtra

Mahesh Thakkar
Director,
Birbal Sahni Institute of Paleosciences,
Lucknow, Uttar Pradesh

Ramdayal Singh
Scientist/Engg E,
Space Applications Centre (SAC),
ISRO, Ahmedabad, Gujarat

Satish Sangode
Professor,
Department of Geology,
Savitribai Phule Pune University,
Pune, Maharashtra

*Author for correspondence
E-mail: adiradhu@gmail.com